RSC Advances

PAPER

Cite this: *RSC Adv.*, 2022, **12**, 23387

Construction of a photothermal controlled-release microcapsule pesticide delivery system

Jun Cen,[a] Linhuai Li,[a] Lingling Huang[a] and Guangqi Jiang *[ab]

This study aimed to achieve the controlled-release of bioactive ingredients in microcapsule pesticide delivery systems. A photothermal controlled-release microcapsule pesticide delivery system was constructed using chitosan and polydopamine (PDA) as the wall materials to encapsulate avermectin. All the prepared microcapsules were characterized by the methods of optical microscopy, scanning electron microscopy, transmission electron microscopy, and Fourier-transform infrared spectroscopy. The slow-release, UV-shielding, photothermal performance, and the nematicidal activity of the prepared microcapsules were also systematically investigated. The results indicated that the prepared microcapsules had excellent slow-release and UV-shielding performance when further encapsulated with the PDA layer relative to those of the non-PDA-encapsulated products. The photothermal sensitivity of the AVM@CS/CMA/PDA composite microcapsule under the irradiation of near-infrared light (NIR) was dramatically enhanced with the photothermal conversion efficiency (η) of 14.93%. Furthermore, the nematicidal activity of the AVM@CS/CMA/PDA composite microcapsule system was effectively improved on exposure to the irradiation of a light-emitting diode (LED) full-spectrum light. The strategies used in this study for developing the photothermal controlled-release pesticide delivery system might play an important role on improving utilization of pesticides.

Received 26th July 2022
Accepted 10th August 2022

DOI: 10.1039/d2ra04672e

rsc.li/rsc-advances

1 Introduction

Pesticides, such as avermectin (AVM), having good insecticidal activities, were commonly used in agriculture to protect agricultural products from the damage caused by pests.[1,2] The structure of avermectin is shown in Fig. 1. The overuse of pesticides not only increases the costs of agricultural products but also has potential risks to human beings and the environment.[3–5] Many pesticides are easily oxidized and photodegradable, leading to their overuse during crop growth.[6] Microencapsulation is a good way to achieve slow and controlled-release of agrochemicals in modern agriculture, effectively reducing the overuse of pesticides in crop growth.[7,8] Nowadays, microcapsule pesticides with stimulus-responsive performance for pH value,[9,10] temperature,[11] and enzymes[12,13] have been widely developed to investigate their controlled-release performance and future application prospects in agriculture. Among these controlled-release pesticide delivery systems, the photothermal controlled-release microcapsule pesticides can not only achieve controlled-release of pesticides, but also be easily applied in current agricultural production systems considering the flexibility of application and the low costs of external light regulation.[14–19] The selection of the photothermal agents is highly crucial in the construction of such photothermal controlled-release pesticide delivery systems. The photothermal agents can absorb light and effectively convert light energy into heat energy, resulting in the rise of temperature of the system and thus stimulating the release of pesticides in such a system.[20–22] To date, few photothermal controlled-release pesticide delivery systems have been reported because the common photothermal agents, such as gold nanorods, graphene, and so forth, with high costs and the shortcoming of difficult degradation, are mostly unsuitable for constructing

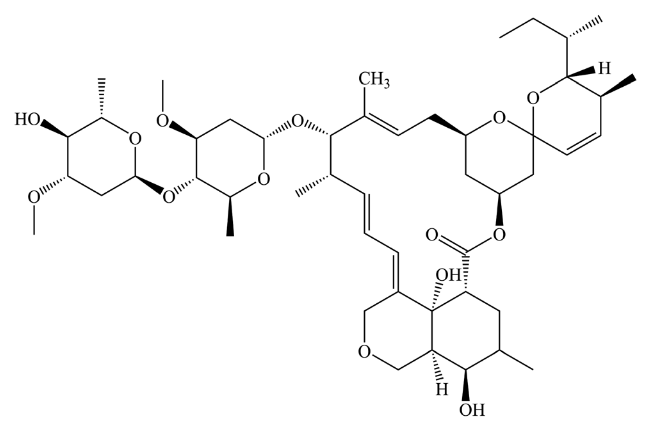

Fig. 1 Structure of avermectin.

[a]College of Chemistry and Chemical Engineering, Guizhou University, Guiyang, China. E-mail: gqjiang@163.com

[b]State Key Laboratory Breeding Base of Green Pesticide and Agricultural Bioengineering, Key Laboratory of Green Pesticide and Agricultural Bioengineering, Ministry of Education, Guizhou University, Guiyang, China

pesticide delivery systems for vast agricultural application.[23–26] Polydopamine (PDA) possesses a photothermal conversion efficiency of 40%, and the virtues of low cost, easy fabrication, biocompatibility, and biodegradability. PDA has been applied in photothermal therapy and near-infrared light (NIR) controlled-release systems as a desirable photothermal agent.[27–29] Furthermore, it can spontaneously attach to virtually all types of inorganic and organic surfaces by oxidative self-polymerization of dopamine (DA) in a weakly alkaline solution.[30–32] Some similar theoretical studies were reported in the literature.[33,34]

In this study, we attempted to construct photothermal controlled-release microcapsule delivery systems using chitosan and PDA as the wall materials to encapsulate avermectin. Fig. 2 illustrates the detailed fabrication process of the pesticide delivery system. As shown in Fig. 2, avermectin was first encapsulated with chitosan by the emulsified cross-linking method. Subsequently, the PDA layer was deposited on the surface of the chitosan layer of the microcapsule *via* oxidative self-polymerization of DA in a weakly alkaline solution (pH = 8.5). After being encapsulated with PDA, the prepared microcapsule systems showed excellent slow-release, UV-shielding, and photothermal sensitivity compared with non-PDA-encapsulated products. Indoor toxicity experiments on the effects of these microcapsule delivery systems on the nematicidal activity showed that these PDA-encapsulated systems accelerated the release of the AVM, resulting in a significant increase in their nematicidal activities under irradiation of a light-emitting diode (LED) plant light. These results indicated that the microcapsule pesticide delivery system might have great application potential in agriculture for the effective utilization of pesticides.

2 Materials and methods

2.1 Materials

Avermectin (AVM, 97 wt%) was provided by Hebei Veyong Biochemical Co. (Hebei, China) and used as received. Chitosan (CS, molecular weight 2×10^5 Da, deacetylation degree ≥ 85%) was supplied by Shandong Luhai Lansheng Biotechnology Co., Ltd (Shandong, China). Dopamine (DA, 98%) was acquired from Shanghai Boer Chemical reagents Co., Ltd (Shanghai, China). Agricultural emulsifier 600# was bought from Shandong Yusuo Chemical Technology Co., Ltd (Shandong, China). Cinnamaldehyde (CMA), cyclohexanone, methanol, and *n*-hexane, as analytical reagents, were bought from the Aladdin Industrial Corporation (Shanghai, China).

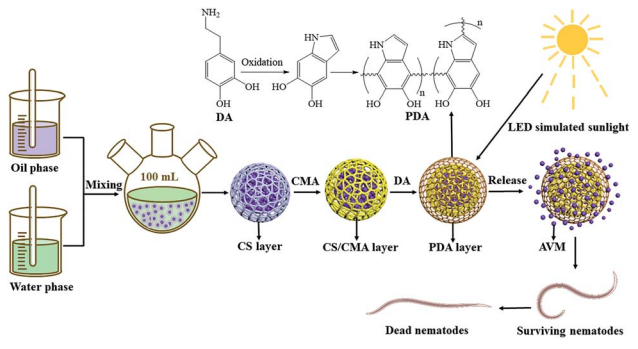

Fig. 2 Fabrication process and controlled release of the pesticide delivery system.

2.2 Preparation of microcapsules

2.2.1 Preparation of AVM@CS microcapsules. 1% (w/w) chitosan solution was prepared by dissolving chitosan into 2% (v/v) acetic acid aqueous solution at ambient temperature. A water phase was formed by dissolving 1.0 g agricultural emulsifier 600# in 26.0 mL of 1% (w/w) chitosan solution. An oil phase was prepared by dissolving 4.12 g of avermectin in 8.0 g cyclohexanone. The water phase and oil phase were mixed in a three-necked flask with a stirring rate of 500 rpm. Further emulsification for 2 h was conducted to prepare the AVM@CS microcapsule suspension. The loading content (LC) and encapsulation efficiency (EE) were determined to be 9.56% and 97.56% (w/w) for the prepared AVM@CS microcapsule suspension.

2.2.2 Preparation of AVM@CS/PDA microcapsules. 10.0 g of AVM@CS suspension was washed with deionized water and centrifuged three times. The resulting precipitate was dispersed in 20 mL of 50 mM Tris-HCl buffer solution (pH = 8.5). Subsequently, 0.2 g DA was added, and the mixture was stirred at 500 rpm for a further 24 h at room temperature. The PDA film was deposited on the surface of the AVM@CS microcapsule particles by the oxidative self-polymerization of dopamine, and AVM@CS/PDA microcapsule suspension was obtained. The loading content (LC) and encapsulation efficiency (EE) were determined to be 5.16% and 97.96% (w/w) for the prepared AVM@CS/PDA microcapsule suspension.

2.2.3 Preparation of AVM@CS/CMA/PDA microcapsules. According to the aforementioned procedure, the AVM@CS suspension was prepared. Subsequently, 0.2 g cinnamaldehyde in 0.68 g anhydrous alcohol was added to the emulsion dropwise as a cross-linking agent. Then, the pH value of the emulsion was adjusted to 6.0 before being placed in a 25 °C water bath for constant-temperature solidification. Finally, the pH value of the emulsion was adjusted to 7.0. The resulting emulsion was weighed, washed, and centrifuged. The obtained precipitate was encapsulated with 0.2 g DA in 20 mL of Tris-HCl buffer solution to prepare the AVM@CS/CMA/PDA microcapsule suspension. As shown in Fig. 3. The loading content (LC) and encapsulation efficiency (EE) were determined to be 5.45% and 97.64% (w/w) for the prepared AVM@CS/CMA/PDA microcapsule suspension.

2.3 Characterization

2.3.1 Morphological characteristics of microcapsules. A small amount of microcapsule suspension was taken and evenly smeared on a glass slide. The preliminary morphology of the microcapsule was analyzed using an Olympus BX43 optical microscope (OM, Olympus Corporation, Japan). The structure and surface morphology of the microcapsule were recorded

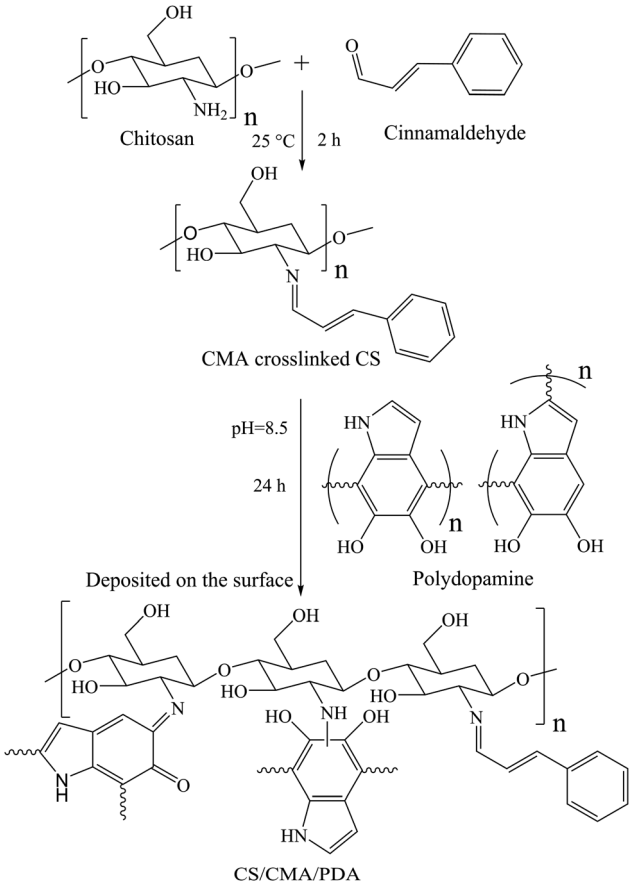

Fig. 3 Synthesis of CS/CMA/PDA wall material.

using an SU8020 scanning electron microscope (SEM, Tianmei Scientific Instruments Co., Ltd, China) and a JEM 2100F transmission electron microscope (TEM, JEM, Japan). The particle size distribution of the microcapsule suspension was measured using a 173Plus Multi-angle particle size analyzer (NY, USA).

2.3.2 Fourier-transform infrared spectroscopy. The Fourier-Transform Infrared (FTIR) spectra of the samples were determined using a VERTEX70 FTIR spectrometer (Brooks, Germany) at a wavelength scan range of 400–4000 cm^{-1}.

2.3.3 Loading content and encapsulation efficiency. Microcapsule suspension (10 mg) was weighed and placed in a 25 mL volumetric flask, and an appropriate amount of methanol was added. The suspension was then ultrasonically disrupted for 2 h and subsequently diluted to 25 mL with a methanol solution to determine the loading content (LC) of avermectin in the microcapsule suspension. Another 10 mg microcapsule suspension was put into a 2 mL centrifuge tube. The suspension was then extracted with hexane three times, and the residual sediment was transferred into a 25 mL volumetric flask. The sediment was ultrasonically disrupted for 2 h and then diluted to 25 mL with a methanol solution for determining the content of avermectin inside of the microcapsules (I). A UV-2700 ultraviolet-visible spectrophotometer (UV-Vis, Shimadzu, Japan) was used to determine the concentration of avermectin in the methanol solution. The concentration of AVM in methanol solution was determined by UV-Vis spectroscopy at 245 nm. Each measurement was analyzed in triplicate. The microcapsule suspension LC and encapsulation efficiency (EE) were calculated using the following equations, respectively.

$$\mathrm{LC} = \frac{m_2}{m_1} \times 100\% \quad (1)$$

$$I = \frac{m_3}{m_1} \times 100\% \quad (2)$$

$$\mathrm{EE} = \frac{I}{\mathrm{LC}} \times 100\% \quad (3)$$

where m_1 is the mass of microcapsule suspension, m_2 is the mass of avermectin in the microcapsule suspension, and m_3 is the mass of avermectin in residual sediment of the microcapsule suspension after being extracted with hexane. (I) is the content of avermectin inside of the microcapsule, and (LC) is the loading content of the prepared microcapsule suspension.

2.3.4 Slow-release performance. The slow-release performance was determined by measuring the cumulative release rate of avermectin from the prepared microcapsule suspensions. Specific amounts of samples were weighed and placed in a dialysis bag with the intercepted molecular weight of 3000, following which the dialysis bag was immersed in a brown reagent vial containing 400 mL of a methanol/water (3/2, v/v) solution. The reagent vial was placed on a shaker and shaken at a rate of 130 rpm. A 2.0 mL of the release medium outside the dialysis bags was collected at different time intervals, and 2.0 mL of the fresh release medium was added to replenish the volume of the system. The concentration of avermectin in the solution was determined by UV-Vis spectrophotometry.

2.3.5 Release kinetics study. The release kinetics of the AVM@CS/CMA/PDA sample was examined as previously described.[35–38] The zero-order, first-order, Higuchi, and Korsmeyer–Peppas equations were used to fit the release curve of avermectin so as to study the release mechanism of the avermectin in the AVM@CS/CMA/PDA pesticide delivery system.

2.3.6 UV-shielding performance. An amount of the microcapsule sample was weighed and added to a methanol/water (20 : 80, v/v) solution in a 250 mL photo-catalytic reactor. Then, the diluted suspension was exposed to a UV lamp (254 nm, 28 W, and 30 μW cm^{-2}) with continuously stirring and kept at room temperature using the recirculating water. At certain time intervals, 1.0 mL of the suspension was withdrawn and transferred to a 10 mL volumetric flask. An appropriate amount of methanol was added, and the suspension was then ultrasonically disrupted for 2 h and subsequently diluted to 10.0 mL. The concentration of avermectin in the solution was determined by UV-Vis spectrophotometry. Further, 1.0 mL of the methanol/water (20 : 80, v/v) solution was added after withdrawing the samples every time to replenish the volume of the system.

2.3.7 Photothermal performance. An aqueous dispersion of the samples with the concentration of 1.0 mg mL^{-1} was irradiated with an 808 nm laser (2.0 W) for 10 min (LASER ON) to evaluate the photothermal performances of AVM@CS,

AVM@CS/CMA, AVM@CS/PDA, and AVM@CS/CMA/PDA pesticide delivery systems. The temperature was measured using a thermocouple thermometer. The temperature change of 1.0 mL aqueous dispersion (1.0 mg mL^{-1}) was recorded as a function of time under continuous irradiation using the 808 nm laser until the solution reached a steady-state temperature, to evaluate the photothermal conversion efficiency of the AVM@CS/CMA/PDA system. Then, the laser was turned off for natural cooling down to room temperature without irradiation (LASER OFF). Subsequently, the additional five lasers ON/OFF cycles were repeated to test the photostability of the AVM@CS/CMA/PDA sample. The photothermal conversion efficiency, η, was calculated using eqn (4)–(7) as follows:[39]

$$\eta = \frac{hs\left(T_{\text{max, sample}} - T_{\text{max, solvent}}\right)}{I\left(1 - 10^{-A_{808}}\right)} \quad (4)$$

$$\tau_S = \frac{m_D c_D}{hs} \quad (5)$$

$$t = -\tau_s \ln(\theta) \quad (6)$$

$$\theta = \frac{T - T_{\text{surr}}}{T_{\text{max, sample}} - T_{\text{surr}}} \quad (7)$$

where h is the heat transfer coefficient, s is the surface area of the container, $T_{\text{max, sample}}$ and $T_{\text{max, solvent}}$ are maximum steady-state temperatures for sample solution and water, respectively. I is the incident laser power (5.7 W cm^{-2}), and A_{808} is the absorbance of the sample at 808 nm. τ_s is the sample system time constant, and m_D and c_D are the mass (1.0 g) and heat capacity (4.2 J g^{-1}) of the deionized water used as the solvent, respectively. θ is a dimensionless parameter, T_{surr} is the ambient temperature of the surroundings, and T is a temperature for sample solutions at a constant cooling time (t). τ_s could be determined by applying the linear time data from the cooling period *versus* $\ln(\theta)$.

2.3.8 Nematicidal activity. According to the published literature,[40] the AVM@CS/CMA/PDA sample was diluted with deionized water into stock solutions and then diluted to a series of concentrations (0.2, 0.4, 0.8, 1.6, 3.2, and 6.4 mg L^{-1}). Subsequently, 200 μL of the sample solution was mixed with 200 μL of pine wood nematode suspension (containing an average of 120 freshly second-stage juveniles) in each well of a 48-well culture plate. The nematodes were incubated in a dark environment or under the irradiation of an LED light (SJZX-ZH001, 110 W) with the illuminance of 29 000–31000 Lux. The death rate of the nematodes was calculated after 8 h. Nematodes were regarded as dead when their bodies were straight and did not move after mechanical prodding with a fine needle. Each treatment was repeated four times to ensure the accuracy of the experiment.

3 Results and discussion

3.1 Morphology analysis

The OM images of the AVM@CS, AVM@CS/PDA, AVM@CS/CMA, and AVM@CS/CMA/PDA microcapsules are shown in Fig. 4(a), (c), (e), and (g). The obtained microcapsules were spherical and had good dispersibility. The SEM images of the AVM@CS, AVM@CS/PDA, AVM@CS/CMA, and AVM@CS/CMA/PDA microcapsules are shown in Fig. 4(b), (d), (f) and (h), respectively. Fig. 4(b) shows that the AVM@CS microcapsule particles had a smooth surface and were nonuniform in size. In contrast, AVM@CS/PDA, AVM@CS/CMA, and AVM@CS/CMA/PDA particles had a relatively rough surface. Part of the AVM@CS/CMA and AVM@CS/CMA/PDA particles in Fig. 4(f) and (h) displayed some dents on their surface, accounting for the water loss of the microcapsule samples, which could indirectly demonstrate the core/shell structure of the microcapsule particles.[41–43] The TEM images of the AVM@CS/CMA/PDA sample are shown in Fig. 4(i) and (j). A relatively rough surface was also observed on the TEM images. Comparing Fig. 4(f) with Fig. 4(h) and (j), it was concluded that the overlapping layers of PDA were deposited on the surface of the AVM@CS/CMA microcapsule particles.[44] The particle size distribution of the AVM@CS/CMA/PDA sample is shown in Fig. 4(k). The D_{50} value of the microcapsule particle was 2.85 μm, which is larger than that of the similar IMPDA microcapsules with D_{50} value of 0.97 μm.[30]

3.2 FTIR spectral analysis

As shown in Fig. 5, Fourier-transform infrared (FTIR) spectroscopy was adopted to compare the different compositions of AVM, CS, AVM@CS, PDA, AVM@CS/PDA, AVM@CS/CMA, and AVM@CS/CMA/PDA. On the FTIR spectra of AVM, the CH_3 stretching vibration peaks were exhibited at 2969 cm^{-1} and 2882 cm^{-1},[45] and the characteristic peak of C=O was seen at 1734 cm^{-1}.[46] The characteristic peaks of AVM obviously appeared in the spectrum of AVM@CS, AVM@CS/PDA, AVM@CS/CMA, and AVM@CS/CMA/PDA, suggesting that the characteristics of the encapsulated AVM were not changed after being encapsulated into chitosan and PDA wall materials *via* a physical process. Compared with the spectra of AVM@CS, AVM@CS/CMA and AVM@CS/CMA/PDA microcapsule samples had a strong absorption band at 1633 cm^{-1} and 1626 cm^{-1}, respectively, which was attributed to the stretching vibration of the formed imine bonds (C=N),[47] reflecting the successful cross-linking of cinnamaldehyde with chitosan.[48,49] For PDA, the absorption bands at 1607 cm^{-1} and 1512 cm^{-1} were the characteristic peaks of indole and indoline.[50,51] On the spectrum of AVM@CS/PDA and AVM@CS/CMA/PDA samples, the characteristic peaks of indole and indoline structures were also observed at 1611 cm^{-1} and 1511 cm^{-1}, respectively. These results revealed that the polydopamine layer was successfully deposited on the surface of these microcapsule samples in their encapsulation process.

3.3 Slow-release performance

As shown in Fig. 6(a), the cumulative amount of AVM from AVM and AVM@CS samples was 97.98% and 87.52% after 132 h, respectively. The encapsulation of the chitosan resulted in a relatively slow-release performance for AVM@CS microcapsule. After further cross-linking with cinnamaldehyde

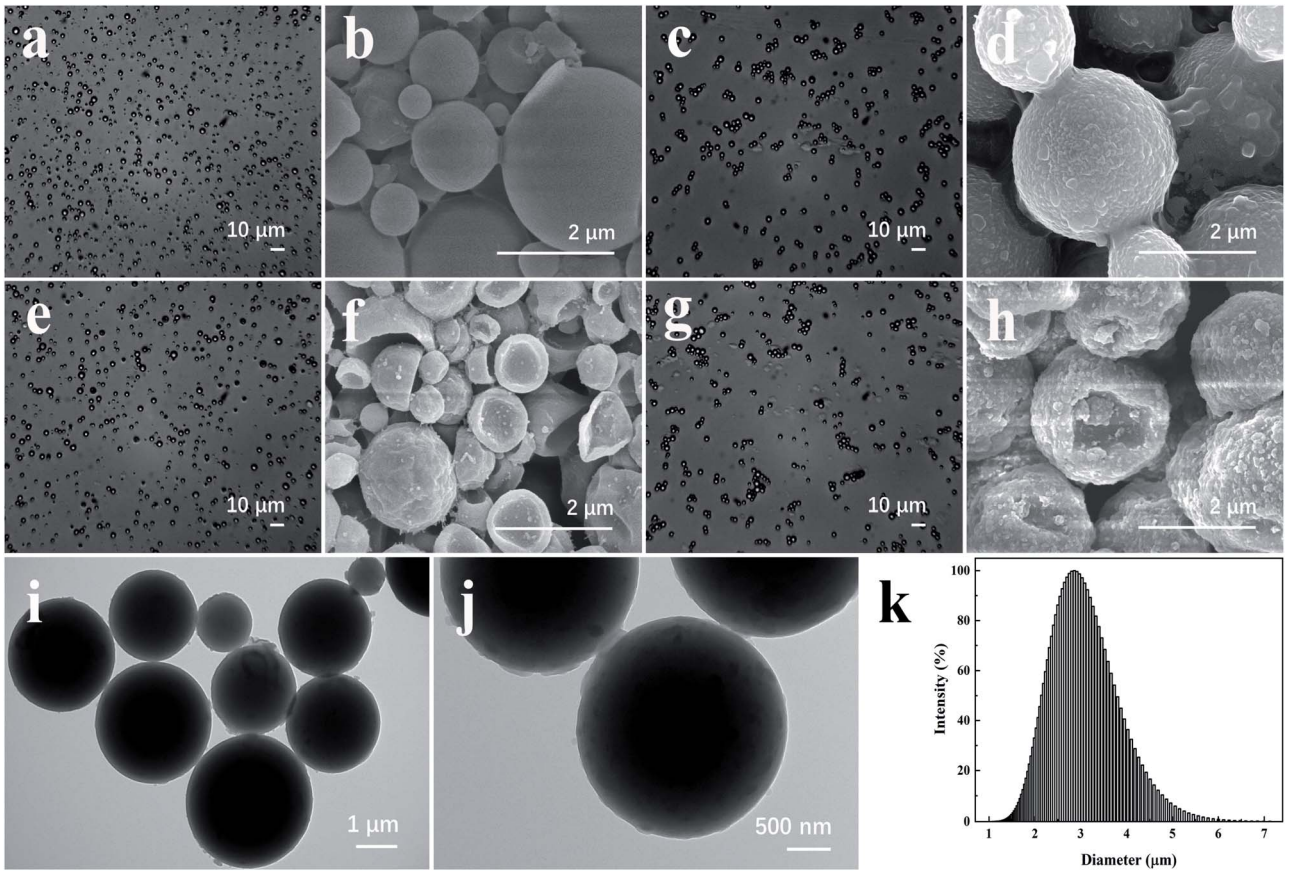

Fig. 4 OM images of microcapsule particles: (a) AVM@CS, (c) AVM@CS/PDA, (e) AVM@CS/CMA, and (g) AVM@CS/CMA/PDA. SEM images of microcapsule particles: (b) AVM@CS, (d) AVM@CS/PDA, (f) AVM@CS/CMA, and (h) AVM@CS/CMA/PDA. TEM images of microcapsule particles (i and j) AVM@CS/CMA/PDA. Particle size distribution of microcapsule particles: (k) AVM@CS/CMA/PDA.

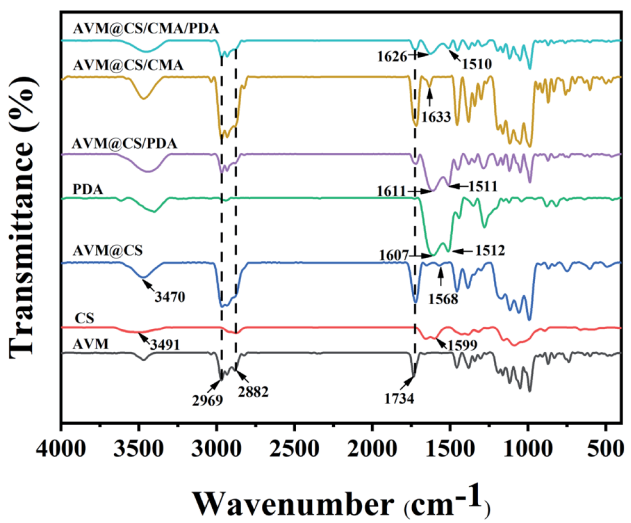

Fig. 5 FTIR spectra of AVM, CS, AVM@CS, PDA, AVM@CS/PDA, AVM@CS/CMA, and AVM@CS/CMA/PDA microcapsules.

(AVM@CS/CMA) or further encapsulation by polydopamine (AVM@CS/PDA), the slow-release performance of the microcapsules was significantly enhanced with the cumulative amount of AVM to 77.47% and 53.20% after 132 h, respectively. The AVM@CS/CMA/PDA microcapsule sample, which was first cross-linked with cinnamaldehyde and then encapsulated with polydopamine, displayed moderate slow-release performance with the cumulative amount of 63.89% after 132 h. We concluded that the order of slow-release performance of these microcapsules was AVM@CS > AVM@CS/CMA > AVM@CS/CMA/PDA > AVM@CS/PDA in methanol/water (3/2, v/v) medium at room temperature. The effect of temperature on the slow-release performance for the AVM@CS/CMA/PDA microcapsule was also investigated. As shown in Fig. 6(b), the cumulative release amount of the AVM after 80 h was 65.56%, 86.61%, and 96.71%, respectively, at 25, 35, and 45 °C, respectively. As shown in Fig. 6(b), the slope of the release curves dramatically increased with the increase in temperature in the initial release stage of 20 h; a higher temperature could result in a higher release rate. Fig. 6(c) shows the slow-release curves of the AVM@CS/CMA/PDA microcapsule sample at pH values of 5, 7, and 9 at room temperature. When the pH value was 5, the cumulative release amount of AVM was 70.30% after 132 h, which was slightly higher than that at the pH value of 7 and 9. This was because PDA usually carried a positive charge due to the protonation of amino groups under acidic conditions. Therefore, the positive charge of the chitosan layers and PDA

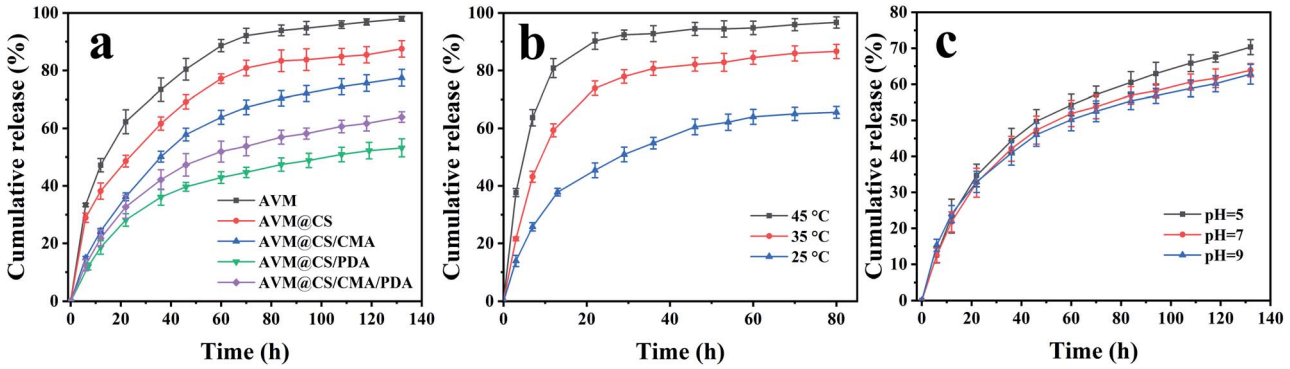

Fig. 6 (a) Release curves of AVM, AVM@CS, AVM@CS/CMA, AVM@CS/PDA, and AVM@CS/CMA/PDA microcapsules. (b) Release curves of the AVM@CS/CMA/PDA in a methanol/water (3/2, v/v) solution at different temperatures. (c) Release curves of the AVM@CS/CMA/PDA in a methanol/water (3/2, v/v) solution with different pH values at room temperature.

layers generated the repulsive force, resulting in the faster release of AVM under acidic conditions.[52]

3.4 Release kinetics of the microcapsule pesticide systems

The commonly used mathematical models for microcapsule slow-release mechanisms are the zero-order, first-order, Higuchi, and Korsmeyer–Peppas equations, where M_t and M_∞ are the cumulative release amounts of the drugs at the time of t and ∞, respectively. Four different kinetic models were used to fit the slow-release curve of the AVM@CS/CMA/PDA microcapsule at pH = 7. The fitting results are shown in Table 1. Among these models, the Korsmeyer–Peppas model had the best results. The R^2 value reached 0.9585, $n = 0.5027$, and $0.43 < n < 0.85$. From the Korsmeyer–Peppas model, the mechanism of drug release was predicted to be non-Fickian diffusion.[53–56]

3.5 Studies of the UV-shielding performance

The UV-shielding performance of the microcapsules was investigated using AVM, AVM@CS, AVM@CS/CMA, AVM@CS/PDA, and AVM@CS/CMA/PDA samples. The decomposition rates of AVM in the microcapsules are shown in Fig. 7. After being irradiated under the UV lamp (254 nm, 28 W, and 30 μW cm^{-2}) for 810 min, the decomposition rate of the AVM sample reached 98.27%. In contrast, after 1290 min of UV irradiation, the decomposition rate of the AVM was 96.23%, 71.67%, 70.54%, and 64.54% for AVM@CS, AVM@CS/CMA, AVM@CS/PDA, and AVM@CS/CMA/PDA samples, respectively. Fig. 7 shows that the decomposition rate of the AVM in the AVM@CS sample was slightly lower than that of the AVM sample, implying that the low UV-shielding effect was achieved only using the chitosan as the wall material for the encapsulation of the AVM. A comparison of the decomposition rate of AVM in AVM@CS, AVM@CS/CMA, and AVM@CS/PDA microcapsules revealed that the AVM@CS microcapsules further cross-linked with cinnamaldehyde or further encapsulated with PDA could effectively enhance the UV-shielding capacity for AVM. These results were in accordance with the published literature.[57,58] As shown in Fig. 7, the prepared AVM@CS/CMA/PDA sample showed the best UV-shielding performance. These results indicated that the AVM@CS microcapsule with further cinnamaldehyde cross-linking and PDA encapsulation could synergistically influence the UV-shielding performance for these pesticide systems.

Table 1 Results of microcapsule release kinetics fitting

Kinetic model	Fitted equation	R^2
Zero-order	$M_t/M_\infty = 0.3618t$	0.8512
First-order	$\ln(1 - M_t/M_\infty) = -0.0066t$	0.9234
Higuchi	$M_t/M_\infty = 5.4767t^{1/2}$	0.9521
Korsmeyer–Peppas	$M_t/M_\infty = 6.1356t^{0.5027}$	0.9585

3.6 Photothermal performance of AVM@CS/CMA/PDA

PDA contains various compact π-stacked microstructures formed by covalent polymerization and non-covalent self-assembly of dihydroxyindole-derived units, and shows broadband absorption properties, PDA layer usually was used as an excellent photothermal conversion material.[59] As shown in

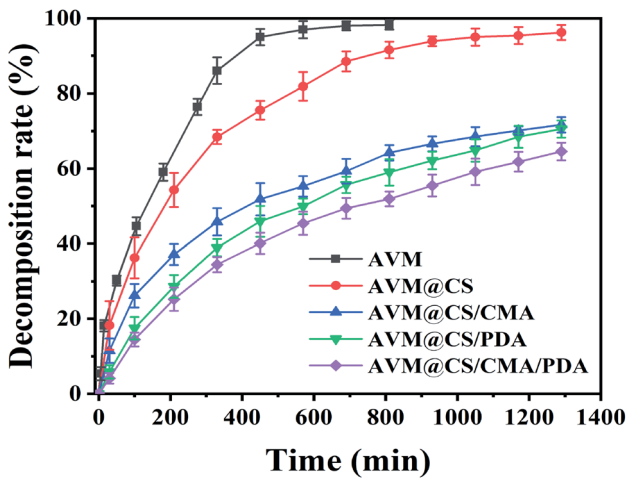

Fig. 7 UV-shielding performance of AVM, AVM@CS, AVM@CS/CMA, AVM@CS/PDA, and AVM@CS/CMA/PDA microcapsules.

Fig. 8(a), the AVM@CS/CMA/PDA microcapsule showed broad absorbance from the Vis to the NIR region; the absorption strength increased with the concentration of the aqueous dispersion of the samples. The temperature elevation profiles for the AVM@CS/CMA/PDA microcapsule at different concentrations of aqueous solutions were measured using laser irradiation at 808 nm. As shown in Fig. 8(b), under laser irradiation for 10 min, the temperature change of AVM@CS/CMA/PDA solution at the concentration of 0.5, 1.0, and 1.5 mg mL^{-1} was up to 27.7, 33.7, and 37.8 °C, respectively, reflecting that AVM@CS/CMA/PDA microcapsule possessed outstanding photothermal performance. Fig. 8(c) shows the photothermal performance of the AVM@CS, AVM@CS/CMA, AVM@CS/PDA, and AVM@CS/CMA/PDA systems and the blank water sample. It clearly indicated that the AVM@CS/PDA and AVM@CS/CMA/PDA systems with the PDA encapsulation had excellent photothermal sensitivity, while no significant change was observed for the blank water sample and the non-PDA-encapsulated products.

To assess the photothermal stability of the AVM@CS/CMA/PDA microcapsule system, 1.0 mL of the AVM@CS/CMA/PDA aqueous solution (1.0 mg mL^{-1}) was irradiated with 808 nm NIR laser for 1080 s, and then the laser was turned off. The temperature of the system was measured using a thermocouple thermometer. The time constant τ_s for the AVM@CS/CMA/PDA microcapsule system heat transfer was calculated by applying the linear time-dependent data collected during the natural cooling. As shown in Fig. 8(d), when irradiated with an 808 nm laser for 1080 s, the temperature increment of the AVM@CS/CMA/PDA aqueous solution was 38.9 °C. As shown in Fig. 8(e), the time constant for heat transfer from the AVM@CS/CMA/PDA system was determined to be 288.7663 s. For the system, $T_{max,\ sample}$ was 55.1 °C, and $T_{max,\ solvent}$ was 20.1 °C, I was 5.7 W cm^{-2}, and A_{808} was 0.395 Abs. τ_s is the sample system time constant, and m_D and c_D are the mass (1.0 g) and heat capacity (4.2 J g^{-1}) of the deionized water used as the solvent, respectively. θ is the dimensionless driving force temperature, T_{surr} is 15.7 °C, and T is the temperature for AVM@CS/CMA/PDA solutions at a constant cooling time (t). Calculated from the aforementioned equations, the photothermal conversion efficiency η of the microcapsule system was 14.93%. The photothermal stability of the AVM@CS/CMA/PDA microcapsule system was examined using laser irradiation every 40 min over five on/off cycles. As shown in Fig. 8(f), the photothermal stability of the AVM@CS/CMA/PDA system was well maintained after five continuous laser-on/laser-off cycles. This revealed that the AVM@CS/CMA/PDA microcapsule system had excellent photothermal stability.[60,61]

3.7 Nematicidal activity

The indoor toxicity experiments for the prepared AVM@CS, AVM@CS/CMA, AVM@CS/PDA, and AVM@CS/CMA/PDA microcapsule systems at the concentrations of 0.2, 0.4, 0.8, 1.6, 3.2, and 6.4 mg L^{-1} AVM were performed, with or without

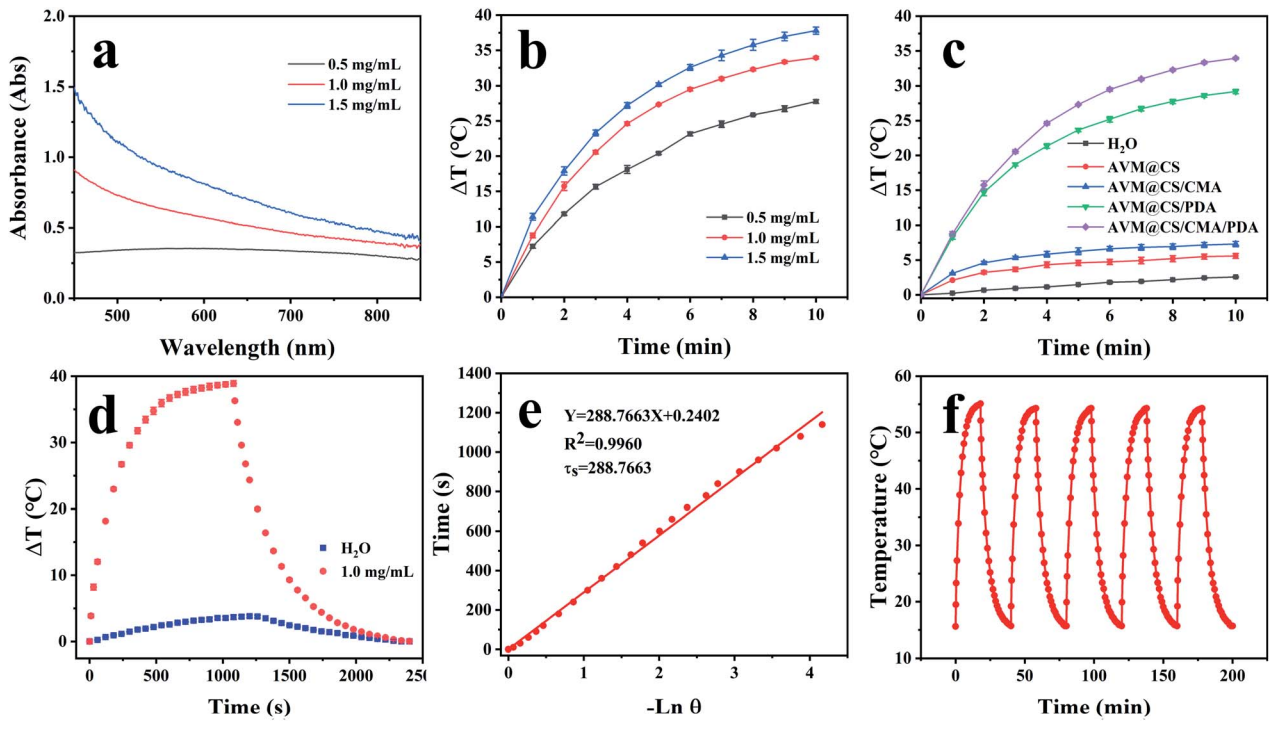

Fig. 8 (a) UV-vis absorption of the AVM@CS/CMA/PDA microcapsule at different concentrations. (b) Photothermal elevation curves of the AVM@CS/CMA/PDA microcapsule at different concentrations. (c) Photothermal elevation curves of the AVM@CS, AVM@CS/CMA, and AVM@CS/PDA, AVM@CS/CMA/PDA microcapsules and H_2O. (d) Irradiation for 1080 s followed by the cooling period; the temperature change in the AVM@CS/CMA/PDA microcapsule system and H_2O. (e) Time constant for heat transfer for AVM@CS/CMA/PDA microcapsule. (f) Photothermal curve of the AVM@CS/CMA/PDA microcapsule with five irradiation on/off cycles.

Table 2 Toxicity of the prepared microcapsule systems on pine wood nematodes with or without the irradiation of LED light

Compound	Exposure duration (h)	Toxicity regression equation	R^2	LC_{50} (95% confidence limit) (mg L^{-1})
AVM@CS	0	$Y = 4.19 + 0.50X$	0.9862	42.04 (16.87–104.76)
AVM@CS/CMA	0	$Y = 4.15 + 0.51X$	0.9897	45.78 (18.99–110.35)
AVM@CS/PDA	0	$Y = 4.09 + 0.52X$	0.9894	54.93 (22.55–133.76)
AVM@CS/CMA/PDA	0	$Y = 4.12 + 0.51X$	0.9899	52.24 (21.06–129.55)
AVM@CS	8	$Y = 4.05 + 0.97X$	0.9936	9.64 (6.64–14.00)
AVM@CS/CMA	8	$Y = 4.15 + 0.93X$	0.9914	8.13 (5.74–7.42)
AVM@CS/PDA	8	$Y = 4.48 + 1.32X$	0.9887	2.46 (2.04–2.97)
AVM@CS/CMA/PDA	8	$Y = 4.53 + 1.29X$	0.9902	2.32 (1.92–2.80)

the irradiation of LED light, to evaluate the practical photothermal controlled-release effect of the systems on pine wood nematodes. The number of deaths of the nematodes under each treatment was determined after 8 h. The LC_{50} values and toxicity regression equations of these microcapsules are presented in Table 2. Without the irradiation of LED light, the order of nematicidal activity was AVM@CS > AVM@CS/CMA > AVM@CS/PDA and AVM@CS/CMA/PDA. These results were in accordance with the research results of the slow-release performance for the prepared microcapsule systems in methanol/water (3/2, v/v) medium. After irradiation with LED light for 8 h, the LC_{50} values for these microcapsule systems obviously reduced. It revealed that the nematicidal activity of all the prepared microcapsule systems could be significantly enhanced under the irradiation of LED light. Furthermore, the PDA-encapsulated products, AVM@CS/PDA and AVM@CS/CMA/PDA systems, had a 22-fold nematicidal activity increase under the irradiation of LED light, while AVM@CS and AVM@CS/CMA systems without PDA encapsulation had 4.36-fold and 5.63-fold increase under the same test condition, respectively.[62,63] Based on these results, it was concluded that the prepared microcapsule systems encapsulated with PDA had excellent photothermal sensitivity and could accelerate the release of AVM in microcapsule delivery systems, resulting in a significant increase in their nematicidal activities under the irradiation of LED light.

4 Conclusions

In this study, a photothermal controlled-release microcapsule delivery system was constructed using chitosan and PDA as the wall materials to encapsulate avermectin. The PDA-encapsulated microcapsule products showed excellent slow-release and UV-shielding performance compared with the non-PDA-encapsulated products. Furthermore, the photothermal sensitivity of the prepared AVM@CS/CMA/PDA composite microcapsule was dramatically enhanced under the irradiation of NIR. Also, the nematicidal activity of the AVM@CS/CMA/PDA pesticide delivery system under the irradiation of a full-spectrum LED light was effectively improved. The surface deposition of the PDA photothermal layer on the microcapsules endowed the pesticide delivery systems with good photothermal and UV-shielding performance. The prepared photothermal controlled-release microcapsule pesticide delivery system might play an important role in improving the utilization of pesticide. Further work on the control efficacies of these microcapsule pesticide delivery systems is undergoing.

Conflicts of interest

The authors report there are no competing interests to declare.

Acknowledgements

This study was supported by the opening foundation of the Key Laboratory of Green Pesticide and Agricultural Bioengineering, Ministry of Education, Guizhou University, Grant No. 2016GDGP0102. We thank EditorBar Language Editing (**https://www.editorbar.com**) for editing this manuscript.

References

1 J. A. Lasota and R. A. Dybas, *Acta Leiden.*, 1990, **59**, 217–225.
2 Food Safety Commission of Japan, *Food Safety*, 2016, **4**, 30–31.
3 P. Nicolopoulou-Stamati, S. Maipas, C. Kotampasi, P. Stamatis and L. Hens, *Front. Public Health*, 2016, **4**, 148.
4 K. Kim, E. Kabir and S. A. Jahan, *Sci. Total Environ.*, 2017, **575**, 525–535.
5 Y. Li, C. Zhang, Y. Yin, F. Cui, J. Cai, Z. Chen, Y. Jin, M. Robson, M. Li, Y. Ren, X. Huang and R. Hu, *Int. J. Environ. Res. Public Health*, 2014, **11**, 3995–4006.
6 E. Chamberlain, H. Shi, T. Wang, Y. Ma, A. Fulmer and C. Adams, *J. Agric. Food Chem.*, 2012, **60**, 354–363.
7 M. L. Alonso, J. M. Laza, R. M. Alonso, R. M. Jiménez, J. L. Vilas and R. Fañanás, *J. Chem. Technol. Biotechnol.*, 2014, **89**, 1077–1085.
8 M. Zhang, Z. Zhu, S. Yuan, S. Wang, C. Yang, P. Dwivedi, T. Si and R. X. Xu, *J. Microencapsulation*, 2019, **36**, 649–658.
9 C. Xu, L. Cao, P. Zhao, Z. Zhou, C. Cao, F. Zhu, F. Li and Q. Huang, *Int. J. Mol. Sci.*, 2018, **19**, 854.
10 C. T. J. Ferguson, A. A. Al-Khalaf, R. E. Isaac and O. J. Cayre, *PLoS One*, 2018, **13**, e201294.
11 D. Xiao, W. Liang, Z. Xie, J. Cheng, Y. Du and J. Zhao, *J. Hazard. Mater.*, 2021, **403**, 123654.
12 M. Guo, W. Zhang, G. Ding, D. Guo, J. Zhu, B. Wang, D. Punyapitak and Y. Cao, *RSC Adv.*, 2015, **5**, 93170–93179.

13 H. Wen, H. Zhou, L. Hao, H. Chen, H. Xu and X. Zhou, *Colloids Surf., B*, 2020, **186**, 110699.
14 Q. Fang, K. Xu, Q. Xiong, Y. Xu, A. Hui and S. Xuan, *Crystengcomm*, 2021, **23**, 6610–6619.
15 Z. Wu, J. Shi, P. Song, J. Li and S. Cao, *Int. J. Biol. Macromol.*, 2021, **183**, 870–879.
16 L. Zhang, S. Ren, C. Chen, D. Wang, B. Liu, D. Cai and Z. Wu, *Chem. Eng. J.*, 2021, **411**, 127881.
17 B. Liu, J. Zhang, C. Chen, D. Wang, G. Tian, G. Zhang, D. Cai and Z. Wu, *J. Agric. Food Chem.*, 2021, **69**, 6981–6988.
18 P. Wang, S. Chen, Z. Cao and G. Wang, *ACS Appl. Mater. Interfaces*, 2017, **9**, 29055–29062.
19 L. Wang, B. Li, F. Xu, Z. Xu, D. Wei, Y. Feng, Y. Wang, D. Jia and Y. Zhou, *Carbohydr. Polym.*, 2017, **174**, 904–914.
20 J. Dong, X. Liu, Y. Chen, W. Yang and X. Du, *J. Colloid Interface Sci.*, 2021, **594**, 20–34.
21 S. Jia, W. Fong, B. Graham and B. J. Boyd, *Chem. Mater.*, 2018, **30**, 2873–2887.
22 M. Mei, B. Bai, D. Zheng, N. Hu and H. Wang, *RSC Adv.*, 2021, **11**, 19395–19405.
23 T. Niidome, *Yakugaku Zasshi*, 2013, **133**, 369–372.
24 J. Liu, C. Detrembleur, M. De Pauw-Gillet, S. Mornet, C. Jérôme and E. Duguet, *Small*, 2015, **11**, 2323–2332.
25 L. Chengnan, Q. Pagneux, A. Voronova, A. Barras, A. Abderrahmani, V. Plaisance, V. Pawlowski, N. Hennuyer, B. Staels, L. Rosselle, N. Skandrani, M. Li, R. Boukherroub and S. Szunerits, *Nanoscale*, 2019, **11**, 15810–15820.
26 J. Li, B. Tang, B. Yuan, L. Sun and X. Wang, *Biomaterials*, 2013, **34**, 9519–9534.
27 R. Zheng, S. Wang, Y. Tian, X. Jiang, D. Fu, S. Shen and W. Yang, *ACS Appl. Mater. Interfaces*, 2015, **7**, 15876–15884.
28 X. Xu, B. Bai, H. Wang and Y. Suo, *ACS Appl. Mater. Interfaces*, 2017, **9**, 6424–6432.
29 D. D. Usta, N. Celebi, F. Soysal, A. S. Y. Saglam, N. Yildiz and K. Salimi, *Colloids Surf., A*, 2021, **611**, 125758.
30 Z. Gao, L. Pang, H. Feng, S. Wang, Q. Wang, M. Wang, Y. Xia and S. Hu, *RSC Adv.*, 2017, **7**, 15762–15768.
31 W. Zheng, H. Fan, L. Wang and Z. Jin, *Langmuir*, 2015, **31**, 11671–11677.
32 H. Li, Y. Zhao and H. Peng, *Prog. Chem.*, 2018, **30**, 1228–1241.
33 M. I. A. Oliveira, R. Rivelino, F. de Brito Mota and G. K. Gueorguiev, *J. Phys. Chem. C*, 2014, **118**, 5501–5509.
34 A. Kakanakova-Georgieva, G. K. Gueorguiev, D. G. Sangiovanni, N. Suwannaharn, I. G. Ivanov, I. Cora, B. Pecz, G. Nicotra and F. Giannazzo, *Nanoscale*, 2020, **12**, 19470–19476.
35 C. G. England, M. C. Miller, A. Kuttan, J. O. Trent and H. B. Frieboes, *Eur. J. Pharm. Biopharm.*, 2015, **92**, 120–129.
36 A. Akbari and J. Wu, *Drug Delivery Transl. Res.*, 2017, **7**, 598–607.
37 J. Huang, H. Lin, B. Peng, Q. Huang, F. Shuai and Y. Xie, *AAPS PharmSciTech*, 2018, **19**, 2144–2154.
38 P. Costa and J. M. Sousa Lobo, *Eur. J. Pharm. Sci.*, 2001, **13**, 123–133.
39 D. K. Roper, W. Ahn and M. Hoepfner, *J. Phys. Chem. C*, 2007, **111**, 3636–3641.
40 Z. Zhou, Y. Gao, X. Chen, Y. Li, Y. Tian, H. Wang, X. Li, X. Yu and Y. Cao, *ACS Appl. Mater. Interfaces*, 2021, **13**, 39066–39075.
41 P. Chaiyasat, Y. Ogino, T. Suzuki and M. Okubo, *Colloid Polym. Sci.*, 2008, **286**, 753–759.
42 P. Chaiyasat, T. Suzuki, H. Minami and M. Okubo, *J. Appl. Polym. Sci.*, 2009, **112**, 3257–3266.
43 D. Supatimusro, S. Promdsorn, S. Thipsit, W. Boontung, P. Chaiyasat and A. Chaiyasat, *Polym.-Plast. Technol. Eng.*, 2012, **51**, 1167–1172.
44 G. Wang, Y. Xiao, H. Xu, P. Hu, W. Liang, L. Xie and J. Jia, *J. Agric. Food Chem.*, 2018, **66**, 11244–11253.
45 D. Zhao, Y. Zhang, L. Lv and J. Li, *Polym. Eng. Sci.*, 2013, **53**, 609–614.
46 Y. Yan, H. Hou, T. Ren, Y. Xu, Q. Wang and W. Xu, *Colloids Surf., B*, 2013, **102**, 341–347.
47 L. Lei, Z. He, H. Chen, D. J. McClements, B. Li and Y. Li, *RSC Adv.*, 2015, **5**, 100114–100122.
48 L. Higueras, G. López-Carballo, R. Gavara and P. Hernández-Muñoz, *Food Bioprocess Technol.*, 2015, **8**, 526–538.
49 H. Chen, X. Hu, E. Chen, S. Wu, D. J. McClements, S. Liu, B. Li and Y. Li, *Food Hydrocolloids*, 2016, **61**, 662–671.
50 D. R. Dreyer, D. J. Miller, B. D. Freeman, D. R. Paul and C. W. Bielawski, *Langmuir*, 2012, **28**, 6428–6435.
51 M. Müller and B. Keßler, *Langmuir*, 2011, **27**, 12499–12505.
52 Z. Shen, X. Zhou, H. Qiu, H. Xu, H. Chen and H. Zhou, *Int. J. Polym. Sci.*, 2018, **2018**, 1–13.
53 Y. Li, H. Li, M. Wei, J. Lu and L. Jin, *Chem. Eng. J.*, 2009, **151**, 359–366.
54 S. Jana, A. Das, A. K. Nayak, K. K. Sen and S. K. Basu, *Int. J. Biol. Macromol.*, 2013, **57**, 129–137.
55 J. Ghitman, R. Stan, A. Ghebaur, S. Cecoltan, E. Vasile and H. Iovu, *Polymers*, 2018, **10**, 579.
56 M. R. Abukhadra, N. M. Refay, A. M. El-Sherbeeny and M. A. El-Meligy, *ACS Omega*, 2020, **5**, 11745–11755.
57 Y. Wang, C. Li, X. Zhang, W. Chen and X. Li, *J. Environ. Sci. Health, Part B*, 2021, **56**, 512–521.
58 L. Dong, X. Liu, Z. Xiong, D. Sheng, C. Lin, Y. Zhou and Y. Yang, *J. Appl. Polym. Sci.*, 2018, **135**, 45746.
59 P. Yang, F. Zhu, Z. Zhang, Y. Cheng, Z. Wang and Y. Li, *Chem. Soc. Rev.*, 2021, **50**, 8319–8343.
60 Q. Duan, J. Wang, B. Zhang, X. Wang, J. Xue, W. Zhang and S. Sang, *Colloids Surf., B*, 2022, **210**, 112247.
61 X. Zeng, M. Luo, G. Liu, X. Wang, W. Tao, Y. Lin, X. Ji, L. Nie and L. Mei, *Adv. Sci.*, 2018, **5**, 1800510.
62 A. Bogucka-Kocka, P. Kołodziej, A. Makuch-Kocka, D. Różycka, S. Rykowski, J. Nekvinda, B. Grüner and A. B. Olejniczak, *Chem. Commun.*, 2022, **58**, 2528–2531.
63 X. Liu, D. Lai, Q. Liu, L. Zhou, Q. Liu and Z. Liu, *Molecules*, 2016, **21**, 1665.